Results in Physics 15 (2019) 102667

Contents lists available at ScienceDirect

Results in Physics

journal homepage: www.elsevier.com/locate/rinp

Corrosion behavior of $Co_xCrCuFeMnNi$ high-entropy alloys prepared by hot pressing sintered in 3.5% NaCl solution

Rui-Feng Zhao[a,b], Bo Ren[b], Bin Cai[a], Zhong-Xia Liu[a,*], Guo-Peng Zhang[a], Jian-jian Zhang[a]

[a] School of Physics and Engineering, Key Lab of Materials Physics, Zhengzhou University, No. 75 Daxue Road, Zhengzhou 450052, PR China
[b] College of Science, Henan Institue of Engineering, No. 1 Xianghe Road, Xinzheng, Zhengzhou 451191, PR China

ARTICLE INFO

Keywords:
High-entropy alloy
Hot pressing sintered
Polarization
EIS
Corrosion behavior

ABSTRACT

$Co_xCrCuFeMnNi$ high-entropy alloys (HEAs) were prepared by vacuum hot pressing sintered. The corrosion behavior has been evaluated using potentiodynamic polarization measurements and electrochemical impedance spectra (EIS). The corrosion current density (i_{corr}) and average corrosion rate (V_{corr}) of the alloys decreased with the increase of Co content. When the Co content increased to 2.0 mol from 0.5 mol, the values of i_{corr} and V_{corr} decreased to 6.95×10^{-6} A cm^{-2} and 0.07 mm year^{-1} from 4.04×10^{-5} A cm^{-2} and 0.43 mm year^{-1}, respectively. EIS results reveal that the thickness and resistance of the passive films of $Co_xCrCuFeMnNi$ HEAs increased with the increasing of Co content, indicating the alloy with high Co content had a good corrosion resistance. The reasons for the improvement of corrosion resistance are related to higher the content of passivation elements and FCC2 phase.

Introduction

In the early 21st century, Yeh and Cantor [1,2] developed a novel alloy concept, that is multiple element alloy system, which are more often called high-entropy alloys (HEAs) by the researchers because of their high configurational entropy. The combination of multi-principle elements usually produces four core effects, namely, high mixing entropy, lattice distortion, sluggish diffusion, and cocktail effect, which results in simple microstructure and good properties [3–8]. Up to now, more and more attentions have been focused on the HEAs for their good properties and extensive application prospects [9–14]. Among the previous reported works, the corrosion behavior of the HEAs is one of the hot spots. Back in year 2005, Chen et al. [15] first studied the electrochemical properties of a non-equal-mole 7-component HEA of $Cu_{0.5}NiAlCoCrFeSi$ in detail. The results indicated that the general corrosion resistance of the HEA was superior to that of 304S in 0.1–1 M NaCl and H_2SO_4 aqueous solutions, but the pitting corrosion resistance in a Cl^- environment was inferior to that of 304S. Thereafter the corrosion behavior of different HEAs has been extensively studied by various processes. In 3.5% NaCl solution, the $CoCrFeNiCu_x$ [16] and $FeCrNiCoB_x$ [17] alloys exhibited a poor corrosion resistance. The former resulted from the galvanic action that caused by the segregation of Cu in interdendrite, while the later was due to the formation of tetragonal $(Fe, Cr)_2B$ that deteriorated the corrosion resistance of the HEA coatings. The effect of Co on the corrosion behavior of $Al_2CrFeCo_xCuNiTi$ HEAs coating in alkaline solution and salt solution has been studied by Qiu [18]. The results shown that the HEA coatings have an excellent corrosion resistance in 1 mol NaOH and 3.5% NaCl solutions, which were not only related to the Co content but also the microstructure. Lee et al. [19] have found that the $Al_xCrFe_{1.5}MnNi_{0.5}$ alloys exhibited a wide passive region and their corrosion resistance degraded as the increase of Al content in acidic environments. However, the anodic treatment can optimize their surface structures and minimize their susceptibility to pitting corrosion [20]. Accordingly, the pitting corrosion resistance of $Al_xCrFe_{1.5}MnNi_{0.5}$ alloys was enhanced. Cui et al. investigated the corrosion behavior of FeCoNiCrAl [21] and FeCoNiCrCu [22] under directional solidification in 3.5% NaCl solution. The results shown that the corrosion resistance of directionally solidified alloys was superior to that of the non-directionally solidified alloys.

The HEAs mentioned above were mainly fabricated by casting methods or laser cladding. The cast alloy and coatings usually have structural defects such as voids, porosity, etc. caused by thermal expansion and contraction [23]. In the present work, $Co_xCrCuFeMnNi$ (x = 0.5, 1.0, 1.5, 2.0 mol) HEAs were fabricated by powder metallurgy technique [mechanical alloying (MA) + vacuum hot pressed sintering (HPS)]. The corrosion behavior of the alloys in 3.5% NaCl solution was investigated using the potentiodynamic polarization method and EIS to

* Corresponding author.
E-mail address: liuzhongxia@zzu.edu.cn (Z.-X. Liu).

https://doi.org/10.1016/j.rinp.2019.102667
Received 11 July 2019; Received in revised form 5 September 2019; Accepted 13 September 2019
Available online 19 September 2019

Table 1
Nominal composition of $Co_xCrCuFeMnNi$ high-entropy alloys (mol).

Alloy number	Alloy	Co	Cr	Cu	Fe	Mn	Ni
Co0.5	$Co_{0.5}CrCuFeMnNi$	0.5	1	1	1	1	1
Co1.0	$Co_{1.0}CrCuFeMnNi$	1.0	1	1	1	1	1
Co1.5	$Co_{1.5}CrCuFeMnNi$	1.5	1	1	1	1	1
Co2.0	$Co_{2.0}CrCuFeMnNi$	2.0	1	1	1	1	1

provide a reference for its further study and application.

Materials and methods

The elemental powders of Co, Cr, Cu, Fe, Mn, and Ni (particle sizes ≤ 75 μm, purity > 99.9 wt%) were used as raw materials to fabricate the dual-phase $Co_xCrCuFeMnNi$ (x = 0.5, 1.0, 1.5, 2.0 mol, named as Cr0.5, Cr1.0, Cr1.5, and Cr2.0, respectively) HEAs. The contents of each element are proportioned according to Table 1. Firstly, the $Co_xCrCuFeMnNi$ HEA powders were synthesized using mechanically alloying [24]. The mixed elemental powders were dry milled 45 h in a high energy planetary ball mill at 300 rpm with a ball-to-powder weight ratio of 10:1 under an argon atmosphere. And then the powders were wet milled 5 h in ethanol. Finally, the bulk $Co_xCrCuFeMnNi$ HEAs were sintered in ZT-25-20Y vacuum hot press furnace. The compacted billets were sintered for 2 h under a pressure of 40 MPa at target temperatures (935–946 °C), and then cooled to room temperature slowly.

The dual-phase structure were investigated through x-ray diffraction (XRD) with a Cu Kα radiation (Bruker D8, λ = 0.15406 nm). Density of the HEAs was measured with Archimedes draining method. Potentiodynamic polarization curves were measured in 3.5% NaCl solution by an electrochemical workstation (CHI660 E) at room temperature, using three-electrode system with the saturated calomel reference electrode (SCE), large-area platinum counter electrode, and the polished HEAs working electrode. The area of 1.2 cm^2 was exposed in the solution. Prior to the measurement, the specimen was maintained for 15 min in the solution to stabilise the open circuit potential (OCP). Then the EIS was carried out at the OCP with a sinusoidal potential amplitude of 10 mV, running from 0.01 to 10^5 Hz. Finally, the potentiodynamic polarization tests were performed at a scan rate of 10 mV S^{-1} from an initial potential of −1.5 V to a final potential of 1.5 V versus the OCP.

Results and discussion

Potentiodynamic polarization

Fig. 1 shows the potentiodynamic polarization curves of the $Co_xCrCuFeMnNi$ HEAs in 3.5% NaCl solution. Limited regions of passivation can be observed on the curves, which indicates a tendency of the alloys to passivate. Table 2 gives the corrosion dynamics parameters obtained by linear fitting. The average corrosion rates (V_{acr}) can be calculated by Eq. (1) [15,25].

$$V_{acr} = \frac{3.27 \times 10^{-3} \times i_{corr} \times EW}{D} \quad (1)$$

where V_{acr} is the average corrosion rate of alloy (in mm $year^{-1}$), EW is the equivalent weight of alloy, i_{corr} is the corrosion current density of alloy (in μA cm^{-2}), and D is the density of alloy (in g cm^{-3}). The D values of Co0.5, Co1.0, Co1.5, and Co2.0 alloys are 7.88, 7.97, 8.06, and 8.07 g cm^{-3}, respectively. EW of the HEAs can be calculated by Eq. (2) [15].

$$EW = \frac{1}{\sum\left(\frac{f_i n_i}{a_i}\right)} \quad (2)$$

where f_i, n_i, and a_i are molar ratio, electrons exchanged, and atomic weight, respectively, of the ith alloying element. From Eq. (2), EW of Co0.5, Co1.0, Co1.5, and Co2.0 alloys are 25.89, 26.15, 26.38, and 26.58, respectively. The values of V_{acr} can be acquired based on Eqs. (1) and (2) and were also listed in Table 2.

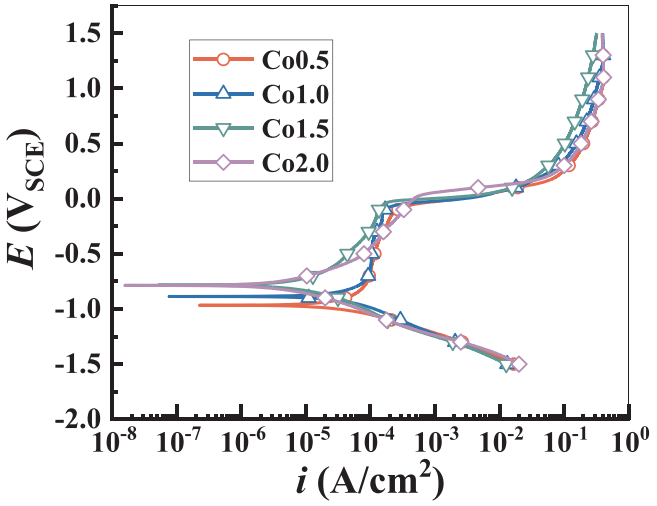

Fig. 1. Potentiodynamic polarization curves of the $Co_xCrCuFeMnNi$ HEAs in 3.5% NaCl solution.

Table 2
Corrosion dynamics parameters of $Co_xCrCuFeMnNi$ HEAs in 3.5% NaCl solution.

Alloys	D (g cm^{-3})	EW	E_{corr} (mV)	i_{corr} (A cm^{-2})	E_{pit} (mV)	V_{acr} (mm $year^{-1}$)
Co0.5	7.88	25.89	−964	4.04×10^{-5}	−91	0.43
Co1.0	7.97	26.15	−888	3.84×10^{-5}	−88	0.41
Co1.5	8.06	26.38	−785	1.11×10^{-5}	−41	0.12
Co2.0	8.07	26.58	−787	6.95×10^{-6}	19	0.07

When the Co content was 0.5 mol, E_{corr} and i_{corr} were −964 mV and 4.04×10^{-5} A cm^{-2}, E_{pit} and V_{acr} were −91 mV and 0.43 mm $year^{-1}$, respectively. As the increasing of Co content, E_{corr} and E_{pit} increases gradually but i_{corr} and V_{acr} decreases. When Co content increased to 2.0 mol, E_{corr} and E_{pit} increased to −787 mV and 19 mV, while i_{corr} and V_{acr} respectively decreased to 6.95×10^{-6} A cm^{-2} and 0.07 mm $year^{-1}$, respectively. The results indicates the corrosion resistance of the $Co_xCrCuFeMnNi$ HEAs improves with increasing Co content.

The corrosion resistance of the alloys is mainly affected by the components when other conditions are the same. In the $Co_xCrCuFeMnNi$ HEAs, the passivation ability of alloying elements declines in sequence from Cr, Ni, Co, Fe, Mn to Cu [26]. It is clear, the Cr, Ni and Co easily form a dense passive film to prevent further corrosion of the alloys. The higher the content of passivation elements, the stronger the corrosion resistance of the alloys. Therefore, the Co2.0 alloy has the best corrosion resistance among the alloys. Due to the strong passivation capacity of Cr and Ni, the formation of Cr and Ni oxide film on the surface of the alloys is effective in protecting the HEAs. The anodic reaction is as follows [27].

$$2Cr + 3H_2O \rightarrow Cr_2O_3 + 6H^+ + 6e \quad (3)$$

$$Ni + 2H_2O \rightarrow Ni(OH)_2 + 2H^+ + 2e^- \quad (4)$$

When the localized impairment of the passive film occurs, pitting corrosion advances rapidly. The localized damage on the passive film usually occurred at weak spots (such as porosities, inclusions, mechanical flaws, etc.) contributed to the transport of ions. At the same time, an anodic region is formed. The reaction is as follows.

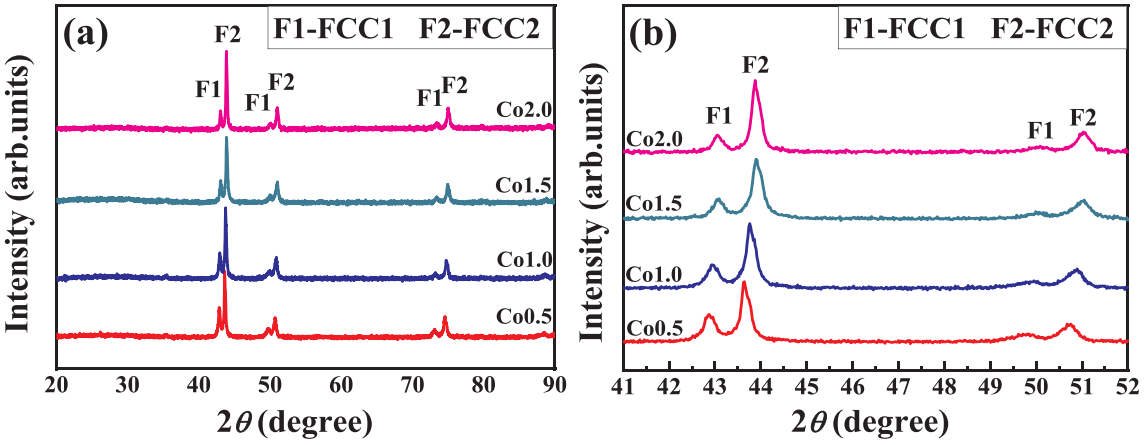

Fig. 2. XRD original patterns (a) and enlarge patterns from 41° to 52° patterns (b) of the sintered $Co_xCrCuFeMnNi$ HEAs.

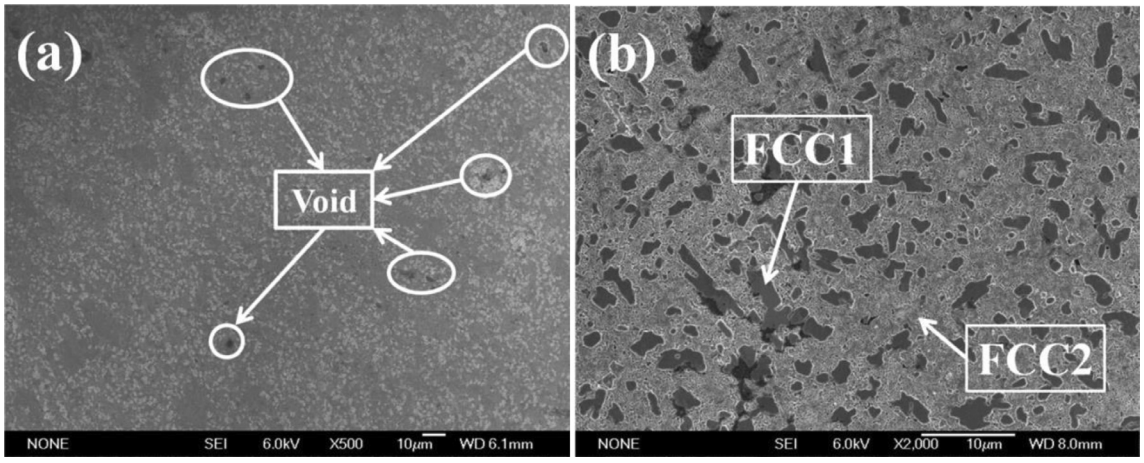

Fig. 3. SEM images of $Co_{2.0}CrCuFeMnNi$ HEAs: (a) low magnification, (b) high magnification.

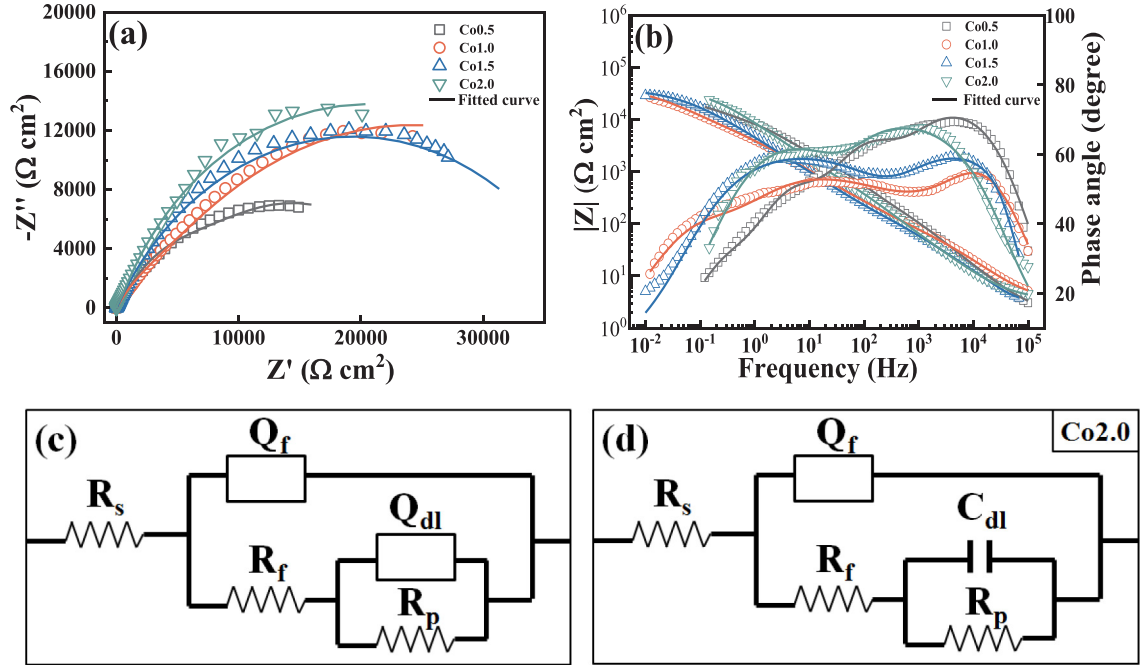

Fig. 4. The (a) Nyqiust and (b) Bode plots and (c, d) the equivalent circuit representative of the electrode interface for the sintered $Co_xCrCuFeMnNi$ HEAs in 3.5% NaCl solution.

Table 3
EIS equivalent circuit parameters for $Co_xCrCuFeMnNi$ HEAs in 3.5% NaCl solution.

Alloys	R_s (Ω cm^2)	Q_f (μF cm^{-2})	α_f	R_f (Ω cm^2)	Q_{dl} (μF cm^{-2})	α_{dl}	R_p (Ω cm^2)
Co0.5	2.37	64.46	0.66	8.51	32.03	0.57	2.64×10^4
Co1.0	3.25	30.16	0.68	19.45	99.31	0.56	4.27×10^4
Co1.5	2.06	2.58	0.90	34.21	100.68	0.98	5.55×10^4
Co2.0	1.09	1.64	0.94	43.98	3.43 (C_{dl})	–	3.20×10^4

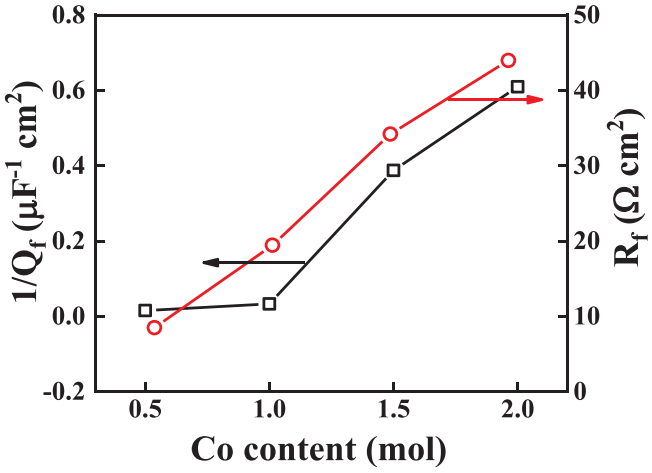

Fig. 5. Relative thickness ($1/Q_f$) and resistance (R_f) of oxide layer as a function of Co content.

$$Cr_2O_3 + 5H_2O \rightarrow 2Cr_2O_4^{2-} + 10H^+ + 6e \quad (5)$$

Additionally, Co enhances the stability of the passive film formed by Cr_2O_3 and $Ni(OH)_2$ through the formation adsorption layer of $Co(OH)_2$ on the surface of the alloys. Therefore, the corrosion resistance of the alloys with high Co content is enhanced. The reaction is as follows.

$$Co + 2H_2O \rightarrow Co(OH)_2 + 2H^+ + 2e^- \quad (6)$$

Phase structure also has an important effect on the corrosion resistance of the alloys. Lee [19] suggested that the corrosion resistance of $CrFe_{1.5}MnNi_{0.5}$ alloy with a FCC structure is superior to that of $Al_xCrFe_{1.5}MnNi_{0.5}$ alloys with a BCC structure. However, The $Co_xCrCuFeMnNi$ HEAs were composed of two face-centered cubic (FCC) solid-solution phases, one was (Fe, Cr)-rich FCC1 phase and the other was (Co, Cu, Ni, Mn)-rich FCC2 phase, as shown in Fig. 2. As the Co content increased, from Fig. 2b, the enhanced peak intensities of the FCC2 phase indicated the relative content of FCC2 phase increased as well. The relative content of FCC2 phases can be estimated by Eq. (7) [28].

$$RC_{FCC2} = \frac{\sum I_{i(FCC2)}}{\sum I_{i(FCC1)} + \sum I_{i(BCC2)}} \times 100\% \quad (7)$$

where $I_{i(FCC1)}$ and $I_{i(FCC2)}$ are the relative intensities (excluding basement) of the ith diffraction peak of FCC1 and FCC2 phases of the alloys, respectively. The relative contents of FCC2 phases for Co0.5, Co1.0, Co1.5, and Co2.0 alloys are 70.7%, 73.7%, 75.8%, and 82.3%.Therefore, the FCC2 phase with more Co element in solid solution is more resistant to corrosion than FCC1 phase. Hsu et al. [16] has studied the corrosion behavior of as-cast $FeCoNiCrCu_x$ HEAs in 3.5% NaCl solution. The corrosion current density of the alloys is between 1.32×10^{-6} and 3.15×10^{-8} A cm^{-2}. However, the corrosion current density of SPS-ed $FeSiBAlNiCo_x$ (0.2, 0.8) is about 5×10^{-3} A cm^{-2} [29]. It can be seen that the corrosion current density of as-cast $FeCoNiCrCu_x$ HEAs is about 1–5 orders lower than that of HPS-ed $Co_xCrCuFeMnNi$ and SPS-ed $FeSiBAlNiCo_x$ HEAs at the same corrosion conditions. Indeed, the sintered alloys have more defects (such as voids and porosities), which provide a convenient conditions for corrosion. Fig. 3 shows the microstructure of $Co_{2.0}$ HEAs. Some voids can be observed in the low-magnification image (Fig. 3a), and the FCC1 and FCC2 phases can also be identified from the high-magnification image (Fig. 3b). Compared with as-cast HEAs, therefore, the sintered HEAs have an inferior resistance to corrosion.

Electrochemical impedance spectroscopy

Fig. 4 shows the EIS results of $Co_xCrCuFeMnNi$ HEAs in 3.5% NaCl solution and their equivalent circuit diagrams. Table 3 lists the related parameters of the equivalent circuit diagrams, where R_s, R_f, and R_p are the resistances of the solution, oxide layer, and absorption layer, Q_f and Q_{dl} are the capacitances of constant phase element (CPE) for oxide layer and absorption layer, and C_{dl} is the capacitance of the absorption layer, respectively. The CPE exponent α is a measure of the capacitance dispersion with values between 1 (ideal capacitance) and 0.7 (highly dispersed capacitance, such as at porous electrodes). Based on the Helmholtz model [30], the oxide layer thickness can be expressed as d, the $d = \varepsilon\varepsilon_0 S/Q_f$, where ε_0 is the permittivity of a vacuum (8.85×10^4 F cm^{-1}), ε is the dielectric constant of the medium, and S is the surface area of the electrode. The value of d is proportional to $1/Q_f$ if we assume that the ε and S for all oxide layers are the same. The values of $1/Q_f$ and R_f are presented in Fig. 5 as a function of Co content. It can be seen that the thickness of oxide layers (d) and the resistance of the oxide layers (R_f) decreased with the increasing of Co content. This is reasonable because the thicker the oxide layers, the greater the resistance of the oxide layers. In addition, the CPE exponents α_f and α_{dl} increased as the increase of Co content, which indicates that the oxide film formed on the surface of the alloys with low Co content is more porous, and thus shows relatively poor corrosion resistance.

According to Fig. 4c and d, the Co2.0 alloy reveals a component of capacitance in the equivalent circuit. In previous research, the alloys containing Ni and Co readily form $Ni(OH)_2$ and $Co(OH)_2$, which are aggregated on the surface of the alloys and effectively increase the amount of the ions in the adsorption layers. Therefore, the value of Q_{dl} increases with the Co content. When the Co content is 2.0 mol, the capacitance appears in the equivalent circuit (as shown in Fig. 4d), indicating that the adsorption layers has an ideal status, such as good compactness and homogeneity. It benefits the improvement of corrosion resistance of the alloys.

Conclusions

The corrosion resistance of the $Co_xCrCuFeMnNi$ HEAs in 3.5% NaCl solution increased with the increasing of Co content. The E_{corr}, i_{corr}, and V_{acr} of Co0.5 alloy were -964 mV, 4.04×10^{-5} A cm^{-2} and 0.43 mm year^{-1}, respectively. When the Co content increased to 2.0 mol from 0.5 mol, the values of i_{corr} and V_{corr} respectively decreased to 6.95×10^{-6} A cm^{-2} and 0.07 mm year^{-1}, which indicates that the Co2.0 alloy has the best corrosion resistance among the alloys. Good corrosion resistance for the Co2.0 alloy attributes to higher the content of passivation elements and FCC2 phase. EIS results show that the thickness and resistance of the passive films of $Co_xCrCuFeMnNi$ HEAs increased with the increasing of Co content, indicating the alloy with high Co content has a good corrosion resistance. This is consistent with the results of potentiodynamic polarization.

Acknowledgements

The authors would like to acknowledge the financial support by the Natural Science Foundation of Henan Province (182300410232), the National Natural Science Foundation of China (11974316), the Scientific and Technological Innovation Team of Colleges and Universities of Henan Province (18IRTSTHN005).

Appendix A. Supplementary data

Supplementary data to this article can be found online at https://doi.org/10.1016/j.rinp.2019.102667.

References

[1] Yeh JW, Chen SK, Lin SJ, Gan JY, Chin TS, Shun TT, et al. Nanostructured high-entropy alloys with multiple principal elements: novel alloy design concepts and outcomes. Adv Eng Mater 2004;6(5):299–303.

[2] Cantor B, Chang ITH, Knight P, Vincent AJB. Microstructural development in equiatomic multicomponent alloys. Mater Sci Eng A 2004;375–377:213–8.

[3] Yim D, Kim HS. Fabrication of the high-entropy alloys and recent research trends: a review. Korean J Met Mater 2017;55(10):671–83.

[4] Ren B, Liu ZX, Shi L, Wang MX, Li DM, Cai B. Corrosion behavior of CuCrFeNiMn high entropy alloy system in 1 M sulfuric acid solution. Mater Corros 2012;63(9):828–34.

[5] Kang YB, Shim SH, Lee KH, Hong SI. Dislocation creep behavior of CoCrFeMnNi high entropy alloy at intermediate temperatures. Mater Res Lett 2018;6(12):689–95.

[6] Fu ZQ, MacDonald BE, Monson TC. Influence of heat treatment on microstructure, mechanical behavior, and soft magnetic properties in an fcc-based Fe29Co28Ni29Cu7Ti7 high-entropy alloy. J Mater Res 2018;33(15):2214–22.

[7] Tikhonovsky MA, Salishchev GA, Yurchenko NY, Stepanov ND, Zherebtsov SV. Aging behavior of the HfNbTaTiZr high entropy alloy. Mater Lett 2018;211:87–90.

[8] Yan L, Kai S. Enhanced strength of a mechanical alloyed NbMoTaWVTi refractory high entropy alloy. Mater 2018;11(5):669–77.

[9] Kumar N, Murty KL, Mishra RS, Bourham M, Komarasamy M, Fusco M. Understanding effect of 3.5 wt.% NaCl on the corrosion of $Al_{0.1}$CoCrFeNi high-entropy alloy. J Nucl Mater 2017;495(9):154–63.

[10] Ye Q, Feng K, Li Z, Lu F, Li R, Huang J, et al. Microstructure and corrosion properties of CrMnFeCoNi high entropy alloy coating. Appl Surf Sci 2017;396:1420–6.

[11] Wu CL, Zhang S, Zhang CH, Zhang H, Dong SY. Phase evolution and properties in laser surface alloying of FeCoCrAlCuNi$_x$ high-entropy alloy on copper substrate. Surf Coat Technol 2017;315:368–76.

[12] Tan XR, Zhi Q, Yang RB, Wang FZ, Yang JR, Liu ZX. Effects of milling on the corrosion behavior of Al2NbTi3V2Zr high-entropy alloy system in 10% nitric acid solution. Mater Corros 2017;68(10):1080–9.

[13] Pang JY, Xiong T, Wei XX, Zhu ZW, Zhang B, Zhou YT, et al. Oxide $MnCr_2O_4$ induced pitting corrosion in high entropy alloy CrMnFeCoNi. Materialia 2019;6:100275-1-4.

[14] Rudolf Kanyane L, Patricia Popoola A, Malatji N. Development of spark plasma sintered TiAlSiMoW multicomponent alloy: microstructural evolution, corrosion and oxidation resistance. Results Phys 2019;12:1754–61.

[15] Chen YY, Duval T, Hung UD, Yeh JW, Shih HC. Microstructure and electrochemical properties of high entropy alloys-a comparison with type-304 stainless steel. Corros Sci 2005;47(9):2257–79.

[16] Hsu Y, Chiang W, Wu J. Corrosion behavior of FeCoNiCrCu$_x$ high-entropy alloys in 3.5% sodium chloride solution. Mater Chem Phys 2005;92(1):112–7.

[17] Zhang C, Chen GJ, Dai PQ. Evolution of the microstructure and properties of laser-clad FeCrNiCoBx high-entropy alloy coatings. Mater Sci Technol 2016;32(15/16):1666–72.

[18] Qiu X, Wu M, Liu C, Zhang Y, Huang C. Corrosion performance of $Al_2CrFeCo_xCuNiTi$ high-entropy alloy coatings in acid liquids. J Alloy Compd 2017;708:353–7.

[19] Lee CP, Chang CC, Chen YY, Yeh JW, Shih HC. Effect of the aluminium content of $Al_xCrFe_{1.5}MnNi_{0.5}$ high-entropy alloys on the corrosion behaviour in aqueous environments. Corros Sci 2008;50(7):2053–60.

[20] Lee CP, Chen YY, Hsu CY, Yeh JW, Shih HC. Enhancing pitting corrosion resistance of $Al_xCrFe_{1.5}MnNi_{0.5}$ high-entropy alloys by anodic treatment in sulfuric acid. Thin Solid Films 2008;517(3):1301–5.

[21] Cui HB, Wang Y, Wang JY. Microstructural evolution and corrosion behavior of directionally solidified FeCoNiCrAl high entropy alloy. JOM 2011;3:259–63.

[22] Cui HB, Zheng LF, Wang JY. Microstructure evolution and corrosion behavior of directionally solidified FeCoNiCrCu high entropy alloy. Appl Mech Mater 2011;1326(134):146–9.

[23] Xw Q. Microstructure and properties of AlCrFeNiCoCu high entropy alloy prepared by powder metallurgy. J Alloy Compds 2013;555(12):246–9.

[24] Zhao RF, Ren B, Zhang GP, Liu ZX, Zhang JJ. Effect of Co content on the phase transition and magnetic properties of $Co_xCrCuFeMnNi$ high-entropy alloy powders. J Magn Magn Mater 2018;468:14–24.

[25] ASTM. Standard Practice for Laborator Immersion Corrosion Testing of Metals. PA; 2004.

[26] Zhao MQ, Lei AL. Jinshu De FuShi Yu FangHu (in Chinese). National Defence Industry Press. China; 2014.

[27] Rodriguez AA, Tylczak JH, Gao MC, Jablonski PD, Detrois M, Ziomek-Moroz M, et al. Effect of molybdenum on the corrosion behavior of high-entropy alloys $CoCrFeNi_2$ and $CoCrFeNi_2Mo_{0.25}$ under sodium chloride aqueous conditions. Adv Mater Sci Eng 2018;3016304:1–11.

[28] Zhao RF, Ren B, Zhang GP, Liu ZX, Zhang JJ. Phase transition of as-milled and annealed CrCuFeMnNi high-entropy alloy powder. Nano 2018;13(9):1–11.

[29] Wang W, Li B, Zhai S, Xu J, Niu Z, Xu J, et al. Alloying behavior and properties of FeSiBAlNiCo$_x$ high entropy alloys fabricated by mechanical alloying and spark plasma sintering. Met Mater Int 2018;24(5):1112–9.

[30] Zinola CF, Castro Luna AM. The inhibition of Ni corrosion in H_2SO_4 solutions containing simple non-saturated substances. Corros Sci 1995;37:1919–29.